

Universality in the periodicity manifestations in the non-locally coupled map lattices in the turbulent regime

Tokuzo Shimada, Shou Tsukada

*Department of Physics, School of Science and Technology, Meiji University
Higashi-Mita 1-1-1, Tama, Kawasaki, Kanagawa 214-8571, Japan*

In the turbulent regime of coupled map lattice with non-local interaction the maps systematically form periodic cluster attractors and their remnants by synchronization due to the foliation of periodic windows of the element map. We examine these periodicity manifestations in three types of coupled map lattices in $D = 1, 2, 3$. In the first two, the interaction is all-to-all but the coupling decreases with distance in a power and an exponential law. In the third, the interaction is uniform but cut off sharply. We find that in all three models and in all dimensions periodicity manifests universally from turbulence when the same suppression of the local mean field fluctuation is achieved by the non-local averaging.

05.45.+b,05.90.+m,87.10.+e

1. Introduction

Synchronization of coupled chaotic elements was firstly shown for the chaotic flows in a master-slave relation [1] and the more general forms of synchronizing chaotic flows have been extensively explored [2]. The synchronization occurs in general under a subtle balance between the randomness in the elements and the coherence forced by the interaction among them. In order to explore various phases of synchronization in complex systems of many chaotic elements, the coupled map lattice (CML) provides us with a concise testing ground. The CML with the nearest couplings exhibits the spatio-temporal chaos and pattern formation [3,4]. It's another limit, the globally coupled map lattice (GCML) with uniform all to all couplings, truncates the notion of the distance and features succinctly the battle between the order and the disorder [5]. It is a basic model of the network of the chaotic neurons with clustering nature of synaptic connections, and also embodies the basic features of various physical systems such as coupled multi mode lasers, a Josephson junction array, fluid vortices and coupled electric circuits.

The simplest GCML consists of N identical chaotic maps and evolves in discrete time under an interaction via the mean field. It has only two parameters, the nonlinear parameter a of the map and the coupling ε of the averaging all-to-all interaction. Yet it is endowed with a rich variety of phases [5]. If the coupling is taken very large, the maps synchronize in a single chaotic cluster. In the intermediate coupling region, the maps form a few clusters by synchronization and suppress the fluctuation of their mean field. In the 'turbulent regime' — the regime of very small coupling and high non-linearity — no visible clusters are *in general* formed; for most of the coupling values the maps seem evolving randomly by direct observation. However, it has been recently found that, even at the very weak coupling in the turbulent regime, the maps systematically form periodic cluster attractors and their remnant states by synchronization when a certain tuning condition between a and ε is satisfied [6–9]. We call them *periodicity manifestations* (PM's) from the turbulence.

The PM's are intriguing synchronization phenomenon at very weak coupling. In the element map, many periodic windows are embedded in the chaos. The PM's are induced in GCML whose parameters are set along the foliation curves of the periodic windows which run through the parameter space and there the dynamics of maps is reduced by synchronization to that of a respective window. It is known that the turbulent GCML with large N is under unflinching weak coherence (so called hidden-coherence), which induces the violation of law of large numbers in the mean field fluctuation in time [10]. With the new findings of PM's, the turbulent GCML may be regarded as a system which sensitively mirrors the periodic windows of the element maps with the background weak coherence. The amazing fact that even at very weak coupling the maps easily form periodic cluster attractors may have important implications in complex systems of coupled chaotic elements, in particular in the activity of the brain. For instance, an efficient switch between the periodic states via chaos [11] may be realized even in a system in the turbulent phase, provided that at least these PM's are not a particular phenomenon in the most simplified GCML. In this Letter we address ourselves to the question to what extent the PM's depend on the global coupling feature of it.

Related works in the literature may be summarized as follows. In one-dimensional CML it was shown that the hidden-coherence becomes visible with increasing coupling range [12]; the phase diagram of the model at intermediate couplings was examined in [13], and the thermodynamical limit has been analytically investigated [14]. A

two-dimensional CML with couplings following an inverse power law with the distance is shown to share the same phase diagram with GCML [6]. In CML of Ginzburg-Landau oscillators it is shown that the spatial correlator exhibits a power law decay [15,16]. It has been recently shown that in one-dimensional CML with power-law couplings the maximal Lyapunov exponent monotonically increases as the coupling-range varies from global to local [17]. These constitute sure progress in understanding the link between the dynamics of GCML and CML. However, to date, the investigation has been mostly focused on the synchronous chaos and spatio-temporal pattern formation, rather than the formation of periodic clusters, and often limited to a particular dimension. In this Letter we turn our eyes to the PM's and investigate for the first time the variation of them with the change of the coupling-range. We do this extensively in three non-local CML's in dimension $D = 1, 2, 3$. All models interpolate the GCML and the nearest-neighbor CML but in different paths. We show that PM's occur in all models at sufficient non-locality. Furthermore we report that there is a salient universality in PM's. They occur at the same strength, independent from detailed construction and the dimension of the map lattices, when a factor \mathcal{F} , which represents the suppression of the local mean field fluctuation by averaging and calculated from the model parameters, is the same.¹

2. GCML, the periodicity manifestations and the MSD curve

The simplest GCML on the lattice Λ is defined by an evolution equation

$$x_P(t+1) = (1 - \varepsilon)f(x_P(t)) + \varepsilon h_t, \quad P \in \Lambda, \quad (1)$$

with the mean field $h_t \equiv \frac{1}{N} \sum_{Q \in \Lambda} f(x_Q(t))$ and $f(x) = 1 - ax^2$. This is an iteration of a two step process; the independent mapping followed by an interaction via the mean field h_t with an overall coupling ε . By adding (1) over P , we find a relation $\frac{1}{N} \sum_{P \in \Lambda} x'_P = h$;— *the mean field is kept invariant in the interaction*. All the non-local models below respect this invariance rule.

The PM's are organized by the maps by synchronization when the parameters a, ε are in a balance that allows a reduction of the high N -dimensional dynamics to that of the element logistic map in a periodic window at non-linearity b . The balance defines foliation curves on the (a, ε) plane and all GCML on a curve are universally governed by the same window dynamics. The most prominent PM's are induced by the period three window [6]. If GCML is on the foliation curves of the $p3$ window, the maps organize themselves into almost equally populated three clusters, which oscillate mutually in period three — $p3c3$ maximally symmetric cluster attractor (MSCA) [9]. With slightly higher ε at the same a , that is, on the foliation curves from the intermittent region, the maps organize themselves in $p3c2$ cluster attractor. Both $p3$ attractors are formed at any reduction factor ($r \equiv b/a \leq 1$). Generally, for a small reduction ($r \gtrsim 0.95$), maps form $p = c$ MSCA and $p > c$ clusters respectively along the curves of period p window and in the nearby higher ε . In MSCA, the MSD of the mean field fluctuation is minimized due to the high population symmetry and all observed MSCA's are linearly stable [9].² Contrarily, in $p > c$ states, the MSD turns out extremely high due to missing clusters to fulfill the orbits. For a large reduction ($r \lesssim 0.95$), the clusters are no longer formed but their remnants induce the same structure in the MSD — a valley and peak respectively along the curves of a window and in the nearby higher ε . The sequence of the periodic windows in the element map therefore produces a successive valley-peak structure in the MSD curve (a function of ε at a) and a given window induces a pair of a valley and a peak at the dictated position.³ We use below the peak-valley structure in the MSD curve as a succinct representation of PM's.

¹It is in form reminiscent of the universality in the Debye's theory of the specific heat, which takes the same value over various crystals if compared at the same scaled temperature T/Θ_D , where Θ_D may be evaluated from the phonon velocities in the crystals.

²The stability is verified by algebraically solving the eigenvalue problem of the linear stability matrix and free from the numerical trap that occurs in the finite precision iteration at the negative transverse Lyapunov exponent [18]. We have also verified that, for the non-local models in this note not at the GCML limit, the minimum gap among maps in a cluster reaches a plateau from above at $10^{-9} - 10^{-10}$ and no trap occurs.

³The curve for a MSCA with a constant h and produced by a window dynamics at b is given $(a, \varepsilon)^b(r) = \left(\frac{b}{r}, 1 - \frac{ry^*}{2} - \sqrt{r(1 - y^*) + \left(\frac{ry^*}{2}\right)^2} \right)$, where $y^*(b)$ is the time average of the single map orbit at non-linearity b .

3. Non-locally coupled map models

3.1. A power law model: POW_α

As an extension of GCML let us consider a model

$$\begin{aligned} x'_P &= (1 - \varepsilon)f(x_P) + \varepsilon h_P, \quad P \in \Lambda \\ h_P &\equiv \sum_{Q \in \Lambda} W_{PQ} f(x_Q) \\ &= c^{(\alpha)} f(x_P) + d^{(\alpha)} \sum_{\rho=1}^{\rho_{\max}} \frac{1}{\rho^\alpha} \sum_{Q \in \Lambda_\rho(P)} f(x_Q), \end{aligned} \quad (2)$$

where each map couples to other maps via a *local mean field* h_P . The $\Lambda_\rho(P)$ is a sub-lattice of Λ consisting of maps at an equal distance ρ from a site P . For simple analytic estimates below, we approximate it by a set of points on the boundary of a $(2\rho + 1)^D$ square (cube) for $D = 2(3)$. The number of maps in Λ_ρ is then given by $n_\rho = 2, 8\rho, 24\rho^2 + 2$ for $D = 1, 2, 3$ respectively. We impose the periodic boundary condition and the maximum ‘radius’ of Λ_ρ is given by $\rho_{\max} = (N^{1/D} - 1)/2$. As a requisite the weights W_{PQ} in h_P must add to one; $\sum_Q W_{PQ} = 1$. This, with the reciprocity $W_{PQ} = W_{QP}$, leads to an important relation $\frac{1}{N} \sum_{P \in \Lambda} h_P = h$;— *the average of the local mean fields is nothing but the mean field of the whole system*, which holds at any step of the iteration. This in turn guarantees the above invariance rule. From $\sum_Q W_{PQ} = 1$, it follows that

$$c^{(\alpha)} + d^{(\alpha)} S^{(\alpha)} = 1, \quad S^{(\alpha)} \equiv \sum_{\rho=1}^{\rho_{\max}} \frac{n_\rho}{\rho^\alpha}. \quad (3)$$

Let us make (2) into a model which interpolates the GCML and the nearest neighbor CML. In order to match with GCML at $\alpha = 0$, the coefficient must be $c^{(0)} = d^{(0)} = 1/N$. In order to match with the nearest neighbor CML

$$x'_P = f(x_P) + \frac{\varepsilon}{n_1 + 1} \left(\sum_{Q \in \Lambda_1(P)} f(x_Q) - n_1 f(x_P) \right) \quad (4)$$

at $\alpha \rightarrow \infty$, the coefficients must be $c^{(\infty)} = d^{(\infty)} = 1/(n_1 + 1)$. In both limits, $c = d$. Therefore, we set $c^{(\alpha)} = d^{(\alpha)}$ for all α as the simplest interpolation. Normalizing the couplings by (3), we obtain a one parameter extension of GCML, POW_α , with the local mean field

$$h_P = \frac{1}{1 + S^{(\alpha)}} \left(f(x_P) + \sum_{\rho=1}^{\rho_{\max}} \frac{1}{\rho^\alpha} \sum_{Q \in \Lambda_\rho(P)} f(x_Q) \right). \quad (5)$$

We show in Fig. 1 and 2 the result of our extensive analysis of the MSD of the time series of the mean field h_t in POW_α . In Fig. 1 the MSD is shown as a surface plot over the α, ε plane. The surface is constructed for each D by $100(\varepsilon) \times 50(\alpha)$ measured points over the time interval $t = 10^3 - 2 \times 10^3$. We have also taken the same amount of data for other two models below. As noted in the previous footnote our analysis is immune from numerical trap. The MSD curve at $\alpha = 0$ is that of GCML and exhibits the foliation of various windows at full strength [9]. The PM’s diminish with increasing α most quickly in $D = 1$ and it is prolonged in higher dimensions. Apart from this, the three surfaces are remarkably similar each other; if one picks a certain MSD curve at an α in, say, $D = 1$, one can also find the same curve in $D = 2, 3$ at some α' and α'' . This was for us the first clue to the universality in PM’s, which predicts the latter from α .

By the strength of PM’s the α interval may be divided into three typical regions (I,II,III) and for a closer analysis we have also chosen eight marking points (a-h), which are indicated in both figures. In Fig. 2 we compare the phases in $D = 1, 2, 3$ with respect to PM’s by a bar-chart diagram and show the MSD curves at the marking points in the insets.

(I) One can observe all PM’s that occur in GCML. From the GCML limit ($\alpha = 0$) up to the point a, the full strength PM’s are produced. The relevant dominant windows are marked on the MSD curve at a, which agrees precisely with the curve in GCML [9]. From a to d, the peak-valley structures, except for that due to $p3$ clusters,

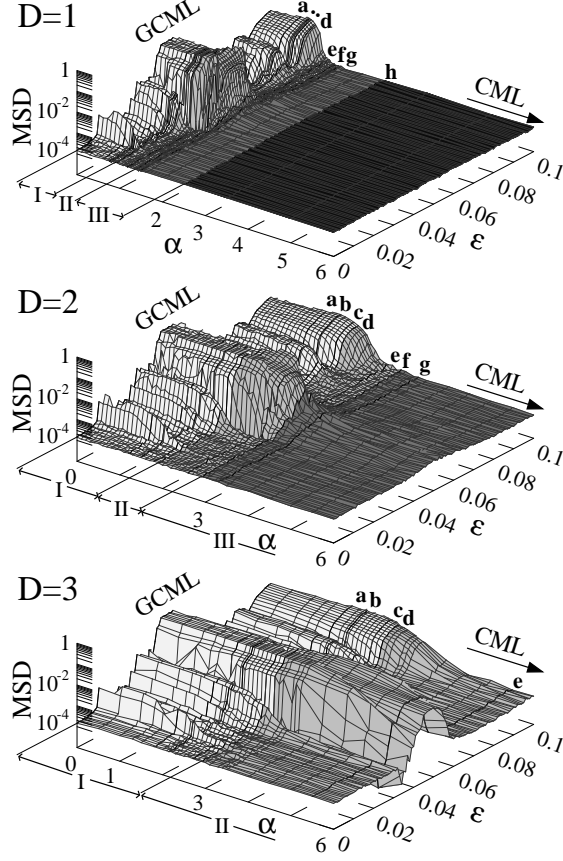


FIG. 1. The MSD surfaces in POW_α over the α, ε plane. $a = 1.90$ and $N = 51^2, 51^2, 13^3$ for $D = 1, 2, 3$ respectively. The MSD curves indicated on the surfaces at the marking points are redisplayed in Fig. 2.

gradually diminish. The peak due to $p5$ window starts diminishing at a and it becomes half-height at b. At c all the sub-dominant peak-valley structures vanish, and even the $p5$ peak vanishes at d.

(II) The region of $p3$ PM's only. It starts from d and the $p3c2$ peak disappears at e. At f, only a broad MSD peak is seen in the MSD curve.

(III) Essentially the region of the hidden coherence. Only broad MSD peak can be seen around the foliation zone of the $p3$ window. At the start of III and near the top of the peak, the temporal correlator of maps decays in a $p3$ motion with exponential envelope. At g, the broad MSD enhancement becomes half-height and the correlator fails to sense the periodicity everywhere. At h, the MSD enhancement disappears.

The transition points T_1, T_2, T_3 between the regions are d, f, h respectively. We note that $\alpha_{T_1} \approx 0.9, 1.9, 2.9$, approximately in the ratios $1 : 2 : 3$ for $D = 1, 2, 3$ respectively.

3.2. A coupled map lattice with exponentially decaying couplings: EXP_{ρ_0}

Similarly, we obtain a model with the local mean field

$$h_P = \frac{1}{1 + S(\rho_0)} \left(f(x_P) + \sum_{\rho=1}^{\rho_{\max}} w_{\rho, \rho_0} \sum_{Q \in \Lambda_\rho} f(x_Q) \right),$$

$$S(\rho_0) \equiv \sum_{\rho=1}^{\rho_{\max}} n_\rho w_{\rho, \rho_0} \tag{6}$$

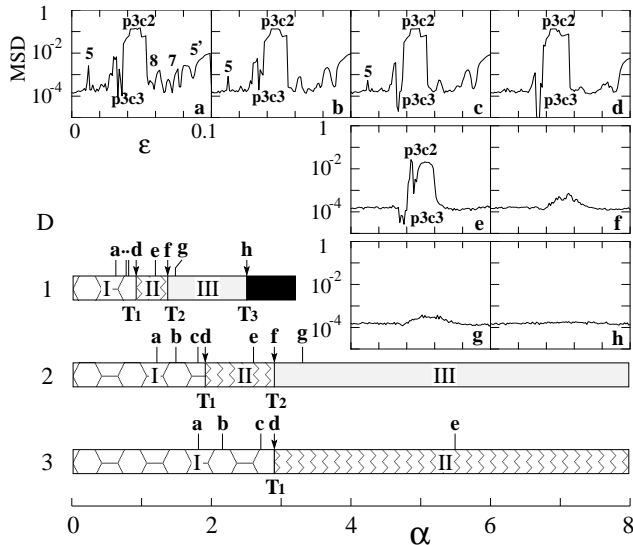


FIG. 2. The bar chart for the PM's in POW_α with $a = 1.90$ and the MSD curves at the eight marking points (a-h). I: full PM's, II: only the $p = 3$ PM's, III: only the hidden coherence.

where $w_{\rho, \rho_0} \equiv \exp(-(\rho - 1)/\rho_0)$ is the exponentially decaying coupling. This reduces to GCML at $\rho_0 \rightarrow \infty$ and the nearest neighbor CML at $\rho_0 \rightarrow 0$. The PM's diminish with *decreasing* ρ_0 via the same patterns of MSD curves.

3.3. A coupled map lattice with an interaction range κ : CML_κ

Above two models maintain all-to-all coupling feature of GCML. Let us now consider a non-local CML with the local mean field

$$h_P = \frac{1}{K} \left(f(x_P) + \sum_{\rho=1}^{\kappa} \sum_{Q \in \Lambda_\rho(P)} f(x_Q) \right). \quad (7)$$

Here $K = (2\kappa + 1)^D$ is the number of maps within a range κ . We find that the PM's diminish with *decreasing* κ , again in the same process as above. Furthermore, we find that remarkably the same PM's occur irrespective to the dimensions if the neighborhood encloses the same number of maps. For instance, the range κ at T_1 is $77-92, 5-6, 2-3$ in $D = 1, 2, 3$ respectively, but the number of maps K within κ is $155 - 185, 121 - 169, 125 - 343$ in $D = 1, 2, 3$. The large error in $D = 3$ comes from the large-step increase of K with κ . Thus for CML_κ we determine the marking points by a refined neighborhood; a set of lattice points Q around P with $\sum_{i=1}^D (\Delta\rho_i)^2 \leq \kappa^2$. In Fig. 3 we show the three regions by a bar chart in terms of K . We find the bars in $D = 1, 2, 3$ agree each other well.

The CML_κ in $D = 1$ was used in an analysis of hidden coherence from the view of 'beat' of mean field [12]. The Fourier power spectrum of h_t is reproduced also in Fig. 3 at $(a, \varepsilon) = (1.99, 0.10)$, which was chosen in [12] to avoid a visible synchronization. Interestingly, the Fourier peaks due to the beat become outstanding in accord with the onset of PM's. The same holds at $(1.90, 0.064)$, which is an equivalent point via the foliation curve.⁴

4. The universality of PM's in non-local models

Let us now put above experimental results in an overview.

⁴The synchronous chaos may disappear at the thermodynamical limit if the coupling range is fixed [14].

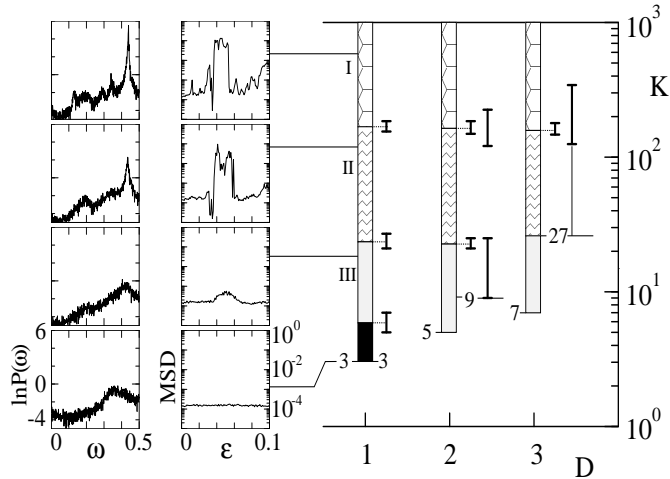


FIG. 3. Right: Bar chart of PM's in CML_κ at $a = 1.90$. I: full PM's, II: only the $p = 3$ PM's, III: only the hidden coherence. The error bars compare the ambiguities in determining the transition points by two types of neighborhood. Center: The MSD curves at the pointed positions. Left: Power spectrum of the mean field at $(a, \varepsilon) = (1.99, 0.10)$ in $D = 1$.

1. *A working hypothesis.* — The difference between GCML and other non-local models is only in the interaction step. In GCML, all the maps contract uniformly to h by a factor $1 - \varepsilon$, while in others a map $f(x_P)$ is contracted to the local mean field h_P which distributes around the overall system mean field h . Therefore, when the variance of $\xi_P \equiv h_P - h$ over the lattice is large in the evolution of the system, some distortion of map configuration must unavoidably be introduced in the interaction step. Contrarily, when the variance is small at each step of the iteration, such a distortion will be avoided and the non-local system may evolve just in the same way with GCML. Thus, it is natural to consider that the deviation from the global limit is controlled by the variance of ξ_P .

The ξ_P is an weighted sum of maps of the form

$$\xi_P = \sum_{Q \in \Lambda} \left(W_{PQ} - \frac{1}{N} \right) f(x_Q). \quad (8)$$

where W_{PQ} is the couplings in (5), (6), (7). If the spatial correlation between the maps are negligible, the variance of ξ_P may be estimated at each time t as

$$\begin{aligned} \langle \xi_P^2 \rangle_\Lambda &\equiv \langle (h_P - h)^2 \rangle_\Lambda \approx \mathcal{F} \langle (f_P - h)^2 \rangle_\Lambda \\ \mathcal{F} &\equiv \sum_Q (W_{PQ})^2 - \frac{1}{N}, \end{aligned} \quad (9)$$

where $\langle \dots \rangle_\Lambda$ denotes the average over the lattice and $\sum_Q W_{PQ} = 1$ is used. The factor \mathcal{F} represents the suppression of the variance of the ξ_P by taking the weighted mean of map values over the lattice Λ . At the global limit, $W_{PQ} \rightarrow 1/N$ and $\mathcal{F} \rightarrow 0$ (strictly no variance). For intermediate couplings and large N the factor $1/N$ may be neglected and \mathcal{F} is solely determined by the couplings. Combined with the above consideration let us propose a working hypothesis that *PM's occur universally in all non-local models when the factor \mathcal{F} is the same and put it under scrutiny below.*

2. *The factor \mathcal{F} in each model.* — In CML_κ , the suppression factor \mathcal{F} is simply $\mathcal{F} = 1/K - 1/N$. This succinctly explains the observation that PM's occur with the same strength at common K in all D and uniformly diminish with decreasing (increasing) K (\mathcal{F}).

TABLE I. The leading N estimate of the \mathcal{F} in POW_α .

D	$\alpha = 0$	$\frac{1}{2}$	1	$\frac{3}{2}$	2	$\frac{5}{2}$	3	$\frac{7}{2}$	∞
1	0	$\ln N/4N$	$\pi^2/12 \ln^2 N$	$\zeta(3)/2\zeta^2(\frac{3}{2})$	$\frac{1}{3}$
2	0	$1/8N$	$\ln N/4N$	$\pi^2/96\sqrt{N}$	$\zeta(3)/2 \ln^2 N$	$\zeta(4)/8\zeta^2(\frac{3}{2})$	$\frac{1}{9}$
3	0	$1/24N$	$1/3N$	$\ln N/4N$	$\pi^2/36N^{\frac{2}{3}}$	$\zeta(3)/48N^{\frac{1}{3}}$	$\pi^4/240 \ln^2 N$	$\zeta(5)/24\zeta^2(\frac{3}{2})$	$\frac{1}{27}$

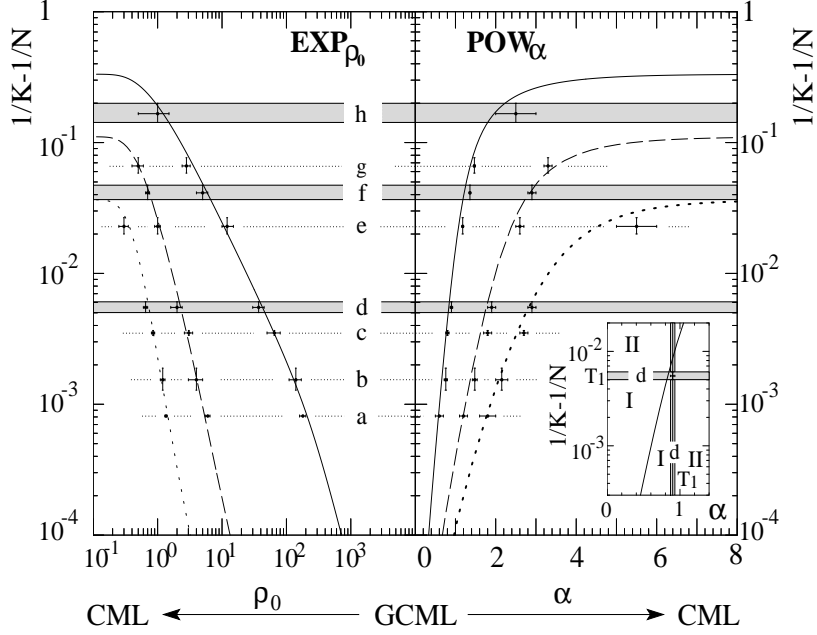


FIG. 4. The comparison between POW_{α} and CML_{κ} (right) and EXP_{ρ_0} and CML_{κ} (left) with respect to eight marked changes (a-h) of the PM's. For $D = 1, 2, 3$ respectively the \mathcal{F}_D is shown by the solid, dashed, and dotted curves and $N = 51^2, 51^2, 13^3$. The inset illustrates the method for the case of d (T_1) in $D = 1$. The α (ρ_0) axis is in the normal (logarithmic) scale.

In POW_{α} the \mathcal{F} is given by

$$\mathcal{F}_D^{(\alpha)} = \frac{1}{(1 + S_D^{(\alpha)})^2} \left(1 + \sum_{\rho=1}^{\rho_{\max}} \frac{n_{\rho,D}}{\rho^{2\alpha}} \right) - \frac{1}{N}. \quad (10)$$

The leading N estimates for $\mathcal{F}_D^{(\alpha)}$ are tabulated in Table. I. We find in particular $\mathcal{F} \approx \log N/4N$ at $\alpha = 1/2, 1, 3/2$ for $D = 1, 2, 3$ respectively. This gives a prediction that the PM's would be universal among $\text{POW}_{\alpha=1/2}^{D=1}$, $\text{POW}_{\alpha=1}^{D=2}$ and $\text{POW}_{\alpha=3/2}^{D=3}$.

This is indeed the case; the full strength PM's, the same with those in GCML, are realized in all the three. The $\mathcal{F}_D^{(\rho_0)}$ in EXP_{ρ_0} may be obtained by substituting $S_D^{(\rho_0)}$ and w_{ρ,ρ_0}^2 to $S_D^{(\alpha)}$ and $1/\rho^{2\alpha}$ respectively.

3. *Overall comparison of the models.*— In Fig. 4 we compare POW_{α} (EXP_{ρ_0}) with CML_{κ} in the right (left). The inset illustrates the case of the transition point $T_1(d)$ in $D = 1$ as an example. The curve is \mathcal{F} for POW_{α} in (10). The measured α at T_1 gives the vertical band taking account for the ambiguity in judging the MSD curve pattern. Hence, the crossing of the curve and the vertical band gives the estimate of \mathcal{F} in POW_{α} at its T_1 in $D = 1$. On the other hand, \mathcal{F} is universal over D in CML_{κ} . The \mathcal{F} at T_1 of CML_{κ} gives the horizontal band, again counting for the ambiguity and averaged over D . Thus, the vertical axis is used for both \mathcal{F} 's, that in POW_{α} and that in CML_{κ} . If both models share exactly the same \mathcal{F} at T_1 , the curve will pass through the crossing junction of the horizontal and vertical bands. In this example, the curve crosses the vertical band slightly above the junction and the estimated \mathcal{F} are $(8.5 \pm 1.5) \times 10^{-3}$ and $(5.5 \pm 0.5) \times 10^{-3}$ in POW_{α} and CML_{κ} respectively. Or, one can predict the α at T_1 in POW_{α} from K at T_1 in CML_{κ} using the \mathcal{F} curve of POW_{α} . The prediction is 0.83 ± 0.02 to be compared with the measured 0.90 ± 0.03 . In the overall comparison, only the junctions are shown by error-bars. We find that the hypothesis remarkably works with respect to all the marking points and in $D = 1, 2, 3$ for \mathcal{F} ranging from 10^{-4} to $O(1)$.

A few remarks are in order.

(a) *The 1:2:3 rule in POW_{α} ;*— The curves in POW_{α} agree approximately with each other after a scale transformation $1 : 1/2 : 1/3$ in α up to $\mathcal{F}_D \approx 2 \times 10^{-2}$. This extends the rule obtained by the leading N calculation. The same strength PM's occur up to the marking point e if α is in the ratio of the system dimensionality, just like the universal

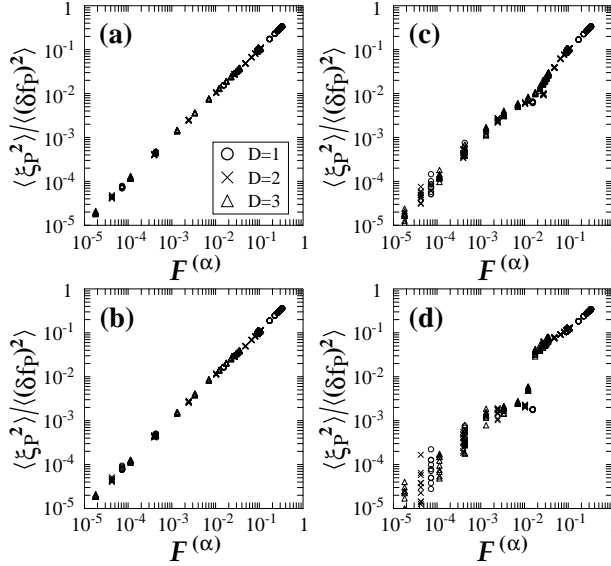


FIG. 5. The ratio $\langle \xi_P^2 \rangle_\Lambda / \langle (f_P - h)^2 \rangle_\Lambda$ averaged over 100 steps versus $\mathcal{F}^{(\alpha)}$, for $\alpha = 0.5 - 8.0$ with $\Delta\alpha = 0.5$ (increasing $\mathcal{F}^{(\alpha)}$) in POW_α . (For $D = 1$, $\alpha = 0.3$ is added.) Points from 10 random starts are overlaid. (a),(b),(c),(d) for $\varepsilon = 0.02, 0.08, 0.0352, 0.045$ respectively.

PM's at the same K in CML_κ .

(b) *Missing transition points*;— The horizontal bands exhibit three transition points observed in CML_κ using refined neighborhood. In other models with the coarse neighborhood, the T_3 is missing in $D = 2$ and both T_2 and T_3 are missing in $D = 3$. (See Fig. 2 for POW_α). The curves of \mathcal{F} explain the difference succinctly; they are constrained by the limiting values $1/3^D$ so they can pass through only the lowest two (one) bands in $D = 2(3)$. We have numerically checked that the missing transition points are retrieved in both POW_α and EXP_{ρ_0} with the refined neighbors.

(c) *Finite- N effect*;— Let us discuss the case of POW_α . As the leading N estimate in Table I shows, \mathcal{F} vanishes at the thermodynamical limit if $\alpha \leq 1, 2, 3$ in $D = 1, 2, 3$ respectively, while for the larger α it approaches a constant. Now, we have already chosen $N > 10^3$, since it is necessary for the PM's (except for $p3$) to occur even in GCML. Thus the marking points a and b are already deep in region I and insensitive to a further increase of N . The points e to h are also insensitive because of the asymptotic limit of \mathcal{F} at a constant. Hence the only place to check the finite size effect is the region near the T_1 and we have verified it ($\mathcal{F} \propto 1/\log^2 N$). For instance, T_1 in $D = 2$ POW_α with $N = 51^2$ is at $\alpha \approx 1.9$ and by replacing N by 10^5 the PM's become into stronger ones, the type around point c in region I, with respect to the $N = 10^5$ GCML⁵, just as predicted.

(d) *Approximation check*;— Our estimate of \mathcal{F} is based on an approximation that the spatial correlation is negligible. We have checked that this is legitimate. Firstly, we note that the even at the formation of cluster attractors such as $p3c3$ MSCA and $p3c2$ states, the spatial distribution of maps does not show any visible clustering. To avoid a confusion we stress that the clustering is in the map values and not in the spatial distribution. We have checked that over the whole turbulent regime of the three models no visible spatial clusters are formed. Furthermore we have directly checked that the estimation in (9) works remarkably well in three models.⁶ The case for POW_α is presented in Fig. 5. The left two boxes are the results for $\varepsilon = 0.02, 0.08$, where no visible synchronization occurs, and the right two for $\varepsilon = 0.0352, 0.045$ where the $p3c3$ and $p3c2$ states are formed respectively. We find that in all dimensions and for all coupling ranges the estimate works remarkably well for \mathcal{F} from 10^{-5} to $O(1)$, which fully covers the range of \mathcal{F} in Fig. 4. The spread of the data points observed in $p3c2$ cluster attractor is due to the different ratios of map

⁵In GCML, the peak-valley structure becomes out-standing with increasing N and remains the same for $N = 10^5 - 10^6$ [9].

⁶Recently an interesting anomalous power-law spatial correlation in the Ginzburg-Landau oscillators is found in [15,16]. For $\varepsilon = 0 - 0.1$ at $a = 1.90$, the range for GCML turbulent regime, the nearest neighbor CML is in fully chaotic phase [4]. But for the non-local CML's, we consider a similar analysis is necessary to confirm our approximation.

populations in the two clusters formed from different initial configurations.

(e) *Inhomogeneous map lattices*;— Even if inhomogeneity is introduced randomly to the non-linearity of maps ($a_P \rightarrow a_P \pm \delta a_P$), all features of PM's discussed in this note are unchanged for $\delta a_P < \delta a = 0.01$. For larger δa the effect is similar to that due to the decrease of non-locality. For instance, with $\delta a = 0.03$, the sequence of marking points starts from the point d for $D = 1, 2, 3$. We have also tested that the PM's occur in non-local CML's with other types of maps with successive windows. Details will be discussed elsewhere.

5. Conclusion

In this note we have focused our attention to the recently found periodicity manifestations in the turbulent regime of GCML. We have conducted an extensive statistical analysis in three non-locally coupled map lattices over $D = 1, 2, 3$ and examined to what extent they depend on the non-locality of the models. We have noted that the essential deviation of the non-local CML from the GCML stems in the variance of the local mean field around the overall mean field. We have analytically estimated the suppression factor \mathcal{F} of the variance under an approximation that the spatial correlation of maps in the turbulence regime is negligible and checked that this \mathcal{F} remarkably agrees with the numerical result. We have found a salient universal that, irrespective of the difference in construction and the dimension of the lattice, the periodicity manifestations occur at the same strength to a good approximation once \mathcal{F} is the same.

Acknowledgements

One of authors (T.S.) especially thanks Wolfgang Ochs for encouragement and reading the manuscript, and Max-Planck Institut für Physik, München for the warm hospitality during his visit. Our thanks also go to Mario Cosenza for communication and Kengo Kikuchi for collaborating with us at the early stage of this work.

-
- [1] L.M. Pecora, T.L. Carroll, Phys. Rev. Lett. 64 (1990) 821.
 - [2] M.G. Rosenblum, A.S. Pikovsky, J. Kurths, Phys. Rev. Lett. 76 (1996) 1804.
H. Fujigaki, M. Nishi, T. Shimada, Phys. Rev. E 53 (1996) 3192.
H. Fujigaki, T. Shimada, Phys. Rev. E 55 (1997) 2426.
G.A. Johnson, D.J. Mar, T.L. Carrol, L.M. Pecora, Phys. Rev. Lett. 80 (1998) 3956.
Z. Liu, Y.-C. Lai, F.C. Hoppensteadt, Phys. Rev. E 63 (2001) 055201.
 - [3] K. Kaneko, Prog. Theor. Phys. 74 (1985) 1033.
J.P. Crutchfield, K. Kaneko, in: Direction in Chaos, ed. H. Bai-lin (World Scientific, Singapore, 1987) p.272.
H. Chaté, P. Manneville, Prog. Theor. Phys. 87 (1992) 1.
 - [4] K. Kaneko, Physica D 34 (1989) 1.
 - [5] K. Kaneko, Phys. Rev. Lett. 63 (1989) 219.
 - [6] T. Shimada, Tech. Rep. IEICE, NLP97-159 (1998) 71.
T. Shimada, Phenomenology of globally coupled map lattice and its extension, Mem. Inst. Sci. Tech., Meiji Univ. 37 (1998) 1, chaos/9810007.
 - [7] T. Shibata, K. Kaneko, Physica D 124 (1998) 177.
 - [8] A. Parravano, M.G. Cosenza, Int. J. Bifurcation Chaos 9 (1999) 2331.
 - [9] T. Shimada, K. Kikuchi, Phys. Rev. E 62 (2000) 3489.
 - [10] K. Kaneko, Phys. Rev. Lett. 65 (1990) 1391; Erratum, Phys. Rev. Lett. 66 (1991) 243.
K. Kaneko, Physica D 86 (1995) 158.
S.V. Ershov, A.B. Potapov, Physica D 106 (1997) 9.
For the ensemble average, the law of large numbers is shown to hold;
A.S. Pikovsky, J. Kurths, Phys. Rev. Lett. 72 (1994) 1644.
 - [11] E. Ott, C. Grebogi, J.A. Yorke, Phys. Rev. Lett. (1990) 1196.
 - [12] S. Sinha, D. Biswas, M. Azam, S.V. Lawande, Phys. Rev. A 46 (1992) 6242.
 - [13] R. Kozma, Phys. Lett. A 244 (1998) 85.
 - [14] P.M. Gade and C-K. Hu, Phys. Rev. E 60 (1999) 4966.
 - [15] Y. Kuramoto, H. Nakao, Physica D 103 (1997) 294.
 - [16] H. Nakao, Chaos 9 (1999) 902.
 - [17] A.M. Batista, R.L. Viana, Phys. Lett. A 286 (2001) 134.
 - [18] T. Shimada and S. Tsukada, in: Proc. of The Sixth Int. Symp. on Artificial Life and Robotics (2001) 242, nlin.CD/0012036.
G. Santoboni, R. Murray, S.R. Bishop, Phys. Lett. A 271 (2000) 358.
A. Pikovsky, O. Popovych, Yu. Maistrenko, Phys. Rev. Lett. 87 (2001) 044102.